

Molecule–surface collision-induced dissociation of internally excited NO_2 on $\text{MgO}(100)$ ☆

H. Ferkel, J.T. Singleton, H. Reisler, C. Wittig

Department of Chemistry, University of Southern California, Los Angeles, CA 90089-0482, USA

Received 16 February 1994; in final form 3 March 1994

Abstract

Collision-induced dissociation (CID) of highly excited NO_2 in the mixed $^2A_1/{}^2B_2$ electronic system has been observed for well characterized $\text{MgO}(100)$ surfaces with parent and product angular resolution at various internal energies. NO state distributions were probed by two-photon, two-frequency ionization, and its yield was found to track the NO_2 absorption spectrum, confirming the CID mechanism. The angular dependence of the NO state distribution indicates that CID occurs following direct inelastic scattering rather than trapping-desorption.

1. Introduction

In molecule–surface collisions involving expansion-cooled samples, the effect of vibrational energy on the scattering of neutral diatomics has been studied both experimentally and theoretically [1–8]. Additionally, the collision-induced dissociation (CID) of expansion-cooled molecules has been examined at hyperthermal translational energies [9–18], the goal being to gain insight into the physical and chemical processes involved in the molecule–surface interactions and to determine the potentials on which the interactions take place. In the work reported here, combinations of translational and internal energies are employed for the first time to investigate the CID of molecules incident on a single crystal surface. NO_2 was chosen because of its absorption features [19] and its long excited state lifetimes (e.g. $\approx 50 \mu\text{s}$) [20], which are needed to achieve high concentrations of

excited molecules striking the crystal surface. It is well known that at high excitation energies, NO_2 is prepared in mixed ${}^2B_2/{}^2A_1$ states having predominantly 2A_1 ground state character. The convenience of detecting NO by resonance-enhanced multiphoton ionization (REMPI) spectroscopy is an additional factor. The relevant electronic states of NO_2 and NO are shown in Fig. 1. The surface used in the experiment was $\text{MgO}(100)$, an inert crystal that should minimize electron-induced processes such as those seen on metal surfaces. Specifically, dissociation will be less likely due to electronic interactions with the crystal. The experiment was performed at various internal energies at an incident translational energy $E_{\text{inc}} = 1940 \text{ cm}^{-1}$ (240 meV), with parent and product angular resolution and typical crystal temperatures of ≈ 400 K. Besides the importance of this experiment to our understanding of activating chemical reactions, as well as intramolecular and crystal excitation, this experiment is also relevant to the recombination of $\text{O}({}^3\text{P})$ with adsorbed NO [21].

☆ Research supported by the Air Force Office of Scientific Research and the Army Research Office.

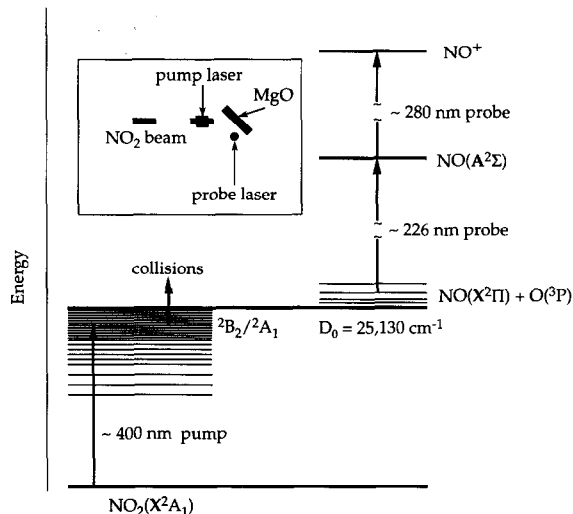


Fig. 1. Schematic energy diagram depicting the CID reaction scheme. Laser excitation prepares internally excited NO_2 with variable energies below dissociation threshold D_0 . Collision of the excited molecule with the surface leads to its dissociation into $\text{NO}(X^2\Pi)$ and $\text{O}(^3P)$; the NO product is probed via REMPI. The inset shows the experimental arrangement of the molecular beam, surface, and laser beams.

2. Experimental

The experiments were carried out in a UHV apparatus that has been described in detail elsewhere [18]. NO_2 samples were purified by several freeze–pump–thaw cycles using an acetone/dry ice slush to pump out NO contamination, which was further reduced by adding equivalent amounts of O_2 . Pulsed expansion of 10% NO_2 and 10% O_2 in 850 Torr H_2 generated a molecular beam with a pulse length of about 100 μs . After passing through a differentially pumped chamber, the beam entered the UHV chamber, with the $\text{MgO}(100)$ crystal in its center. The crystal was cleaved in our laboratory and mounted within 10 min in the UHV chamber, which was then evacuated to 10^{-7} Torr. A 12 h bakeout at 450 K yielded $\approx 10^{-10}$ Torr. Annealing at 1000 K for 2 h in 10^{-5} Torr of O_2 removed surface carbon contamination and oxygen vacancies, and He diffraction showed that the substrate was largely free of defects [22]. The influence of the remaining defects on the results should be negligible, since the incident NO_2 molecules collide mostly with defect-free sites and their residence time on the surface is too short to allow migration to defects (see below).

Highly excited NO_2 states of mixed $^2A_1/{}^2B_2$ character (hereafter referred to as NO_2^*) were prepared ≈ 15 mm in front of the crystal surface by using collimated radiation from an excimer-pumped tunable dye laser system, which entered and left the UHV chamber via quartz windows in the top and bottom of the chamber. The experimental arrangement is shown in Fig. 1. The laser beam was collimated by using a cylindrical lens with the focus line underneath and parallel to the molecular beam axis. The width of the laser beam parallel to the molecular beam was ≈ 4 mm; the energy was ≈ 1 mJ.

The NO CID product was ionized 3–5 mm in front of the surface by using two-frequency REMPI as described before [18]. The probe beams were generated from a Nd:YAG laser pumped tunable dye laser system whose output was frequency-doubled to ≈ 280 nm and Raman shifted to 226 nm. The 226 nm photons ($\approx 6 \mu\text{J}$) excited the $\text{NO } A^2\Sigma^+ \leftarrow X^2\Pi$ system and the $A^2\Sigma^+$ state was then ionized by the more intense 280 nm photons ($\approx 500 \mu\text{J}$). NO^+ ions were extracted and detected with a bare channeltron. The probe beams entered the apparatus from below and were perpendicular to the scattering plane for an in-plane angular resolution of approximately 25° and full integration out of plane (Fig. 1). This arrangement has been described in detail previously [18]. With 280 nm energies $> 700 \mu\text{J}$, ions produced by multiphoton effects in scattered NO_2 molecules were observed. Ionization was also observed when crossing the incident molecular beam with the 280 nm laser beam and was independent of the 226 nm radiation. Similar effects were seen by using only 226 nm radiation, but with much higher energies than were used in our experiments [23]. To minimize these multiphoton effects, experiments were carried out with $\leq 500 \mu\text{J}$ of 280 nm radiation. The dependence of the measured ion signals on the power of the probe laser beams was routinely checked and was always linear. Scattered products were detected near specular angles of 20° and 45° .

To estimate NO_2 rotational temperatures, T_{rot} , use was made of the NO contaminant, whose rotational distribution was measured via REMPI. 99% of the NO was in ${}^2\Pi_{1/2}$ with only the lowest J'' states populated significantly, and rotational temperatures were found to be < 8 K. T_{rot} for NO_2 was assumed to be similar.

Care was also taken to minimize the photodissociation of NO_2 by two-photon absorption of the pump radiation. The absorption of a second photon by NO_2^* was efficient and could be detected by overlapping the pump and probe beams in the incident molecular beam. The pump laser was tuned to an NO_2 level below the dissociation energy ($D_0 = 25130 \text{ cm}^{-1}$ (3.12 eV)), and the NO internal state distribution was probed via two-frequency REMPI. The focus line of the pump laser was then moved towards the molecular beam, and when it reached a critical distance, NO products with high internal energy, characteristic of two-photon NO_2 photodissociation were detected. We found that multiphoton dissociation by the pump could be avoided by keeping the pump fluence at the molecular beam below 10^{16} photons/cm².

The incident molecular beam could be monitored by a quadrupole mass spectrometer (QMS) located at the far end of the UHV chamber, with the crystal moved out of the beam path. Detection of the beam at the H_2 and NO_2 masses revealed a velocity slip between these species, after taking into account the flight time in the QMS. As expected, the slip decreased with increasing backing pressure but was still present at 850 Torr, the pressure used in the CID measurements. At ≈ 50 Torr, even a different velocity between NO_2 and the NO contaminant could be observed, and this was used to determine the relative amount of NO contamination. Fragmentation of NO_2 by the QMS ionizer of course contributed to the late part of the measured NO time-of-flight (TOF) distribution. However, NO impurity occurred as a shoulder on the early side of the TOF spectra, which was not present with freshly purified NO_2 samples.

Since E_{inc} could not be calculated (as opposed to the case of a fully expanded beam), it was measured. The absolute speed of NO_2 in the molecular beam could not be determined by TOF using the QMS, since the time delay between the triggering and actual opening of the nozzle was unknown. Therefore an optical TOF technique was used: NO_2 was dissociated by the pump laser just above D_0 , yielding fragments with nearly the same velocity as the parent, and NO was then probed via REMPI downstream in the molecular beam at distances of 1–10 mm between the pump and probe beams. This yielded an NO_2 speed of ≈ 1000 m/s, corresponding to $E_{\text{inc}} \approx 1940 \text{ cm}^{-1}$ (240 meV).

3. Results and discussion

The bold curve in Fig. 2a shows the NO yield versus excitation energy, $h\nu$, when monitoring $J'' = 6.5$ at $Q_{21} + R_{11}$, with $E_{\text{inc}} = 1940 \text{ cm}^{-1}$, $\theta = 20^\circ$, and $T_s = 400 \text{ K}$. In the present experiments, only $v'' = 0$ levels had appreciable population. The light curve in Fig. 2a shows the $J'' = 6.5$ yield deriving from photodissociation of NO_2 in the molecular beam. The small NO ion signals observed at energies lower than D_0 (which is marked by an arrow at the bottom of Fig. 2) derive from the small fraction of NO_2 molecules in the beam that are rotationally excited. Recently, the CID of NO_2^* by Ar was studied in a crossed mo-

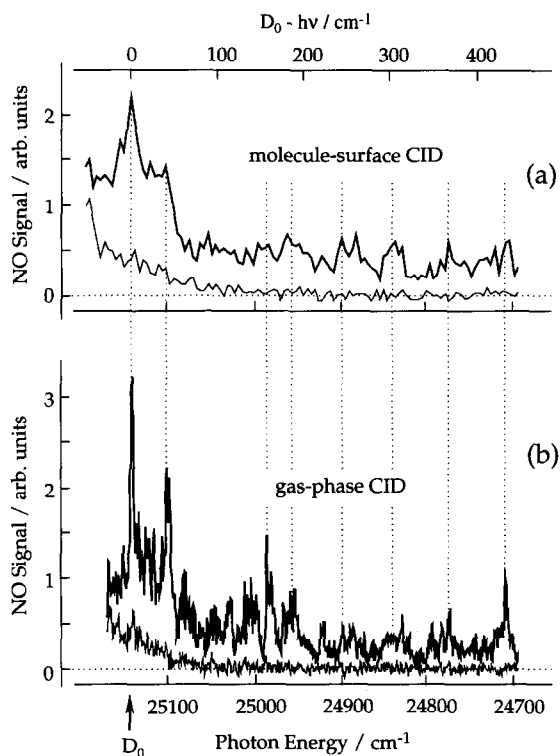


Fig. 2. Relative NO yields versus excitation energy $h\nu$ and excess energy $D_0 - h\nu$. (a) The bold trace is for $\text{NO}_2^* + \text{MgO}(100)$ CID. NO is monitored at $J'' = 6.5$ ($Q_{21} + R_{11}$); $E_{\text{inc}} = 1940 \text{ cm}^{-1}$ (240 meV); $\theta_i = \theta_s = 20^\circ$; and $T_s = 400 \text{ K}$. The light trace is for photodissociation of expansion-cooled NO_2 monitoring NO at $J'' = 6.5$. (b) The bold trace is for $\text{NO}_2^* + \text{Ar}$ gas-phase CID following NO_2 excitation [22]. NO is monitored at $J'' = 5.5$ via P_{11} . The light trace is for photodissociation of expansion-cooled NO_2 monitoring NO at $J'' = 5.5$. The dotted vertical lines highlight the correspondence between the peaks in the gas-phase and molecule-surface CID.

lecular beams arrangement [23], and Fig. 2b shows, for comparison, the corresponding gas-phase CID results obtained at a relative collision energy of 1850 cm^{-1} . The bold curve shows the NO yield when $J''=5.5$ was monitored at P_{11} ; probing $J''=7.5$ at $P_{21}+Q_{11}$ yielded the same features. The light curve in Fig. 2b shows the corresponding $J''=5.5$ background. The molecular beam conditions in both experiments were similar, except that in the crossed beams experiment the carrier was He, with 5% NO_2 and 5% O_2 . All signals are corrected for NO background. The stepping width of the pump laser wavelength was 0.07 nm in the molecule–surface experiment and 0.008 nm in the gas-phase experiment, accounting for the better resolved spectral features in the gas-phase results. The error in our measured CID intensity is about 15% at high yields and 50% at low yields. The large error is due to the NO background in the molecular beam, which scatters with unit efficiency, whereas the CID signal depends strongly on the NO_2 absorption cross section and excited state lifetime. Note that the yields reported here are proportional to concentrations. They do not reflect directly the efficiency with which product states are formed, which requires knowledge of the product-state-specific velocity distributions.

Fig. 2 shows clearly that similar features are observed in the yield spectrum obtained for NO_2^+ CID on $\text{MgO}(100)$ and in the gas phase. Both curves carry the fingerprint of the NO_2 expansion-cooled absorption spectrum [19,23] at the pump excitation wavelengths, confirming the CID mechanism. For example, the peaks in both CID spectra are the same as those observed in LIF spectra of expansion cooled NO_2 [23].

Fig. 3 shows plots of $\ln[N(J'')/(2J''+1)]$ versus NO rotational energy for two different NO_2^+ internal energies and two different values of the angle of incidence, θ_i (i.e. the angle between the molecular beam and the surface normal), with $E_{\text{inc}}=1940 \text{ cm}^{-1}$ and $T_s=400 \text{ K}$. Similar results were obtained with $T_s=700 \text{ K}$. Each of the (a)–(c) entries are averages of three distributions and are corrected for NO background by obtaining NO REMPI spectra with the pump laser on and off. For each set, the NO rotational state distribution from CID was obtained by first generating a rotational distribution for each spectrum, and then subtracting the distributions ob-

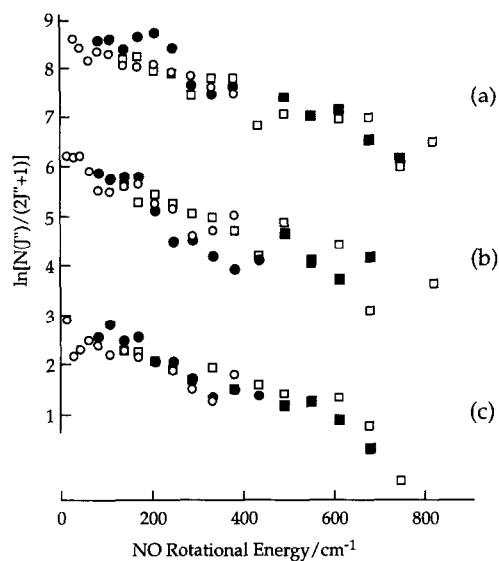


Fig. 3. Plots of $\ln[N(J'')/(2J''+1)]$ versus NO rotational energy for CID of NO_2^+ on $\text{MgO}(100)$ under the following conditions: (a) $\theta_i=\theta_s=20^\circ$, $\lambda=398.62 \text{ nm}$; (b) $\theta_i=\theta_s=20^\circ$, $\lambda=400.18 \text{ nm}$; and (c) $\theta_i=\theta_s=45^\circ$, $\lambda=400.18 \text{ nm}$. $E_{\text{inc}}=1940 \text{ cm}^{-1}$ (240 meV) and $T_s=400 \text{ K}$ in all cases. (●) $Q_{21}+R_{11}$; (○) $Q_{22}+R_{12}$; (■) $P_{21}+Q_{11}$; (□) $P_{22}+Q_{12}$.

tained with the pump laser on and off. As seen in Fig. 3, the lower and upper spin–orbit states, $^2\Pi_{1/2}$ and $^2\Pi_{3/2}$, respectively, have similar populations, with a slightly higher population in the lower spin–orbit state. Overall, the (a)–(c) distributions are similar, and the symbols in Fig. 3 are spread around lines corresponding to a temperature of 450 K. Significant differences are only observed at high J' , i.e. the population in $J''\geq 19.5$ drops more rapidly in (c) than in (a) and (b). Since the population in $J''=21.5$ is close to zero in (c), a corresponding symbol does not appear.

Even with large diameter probe beams close to the surface, TOF measurements of NO fragments were difficult because of small signals and the need to subtract the contaminant scattered NO background. Nonetheless, fragments monitored at the Q_{11} bandhead at different delays revealed an NO ‘packet’ corresponding to the $\approx 4 \text{ mm}$ part of the excited molecular beam, whose velocity was $\approx 1.0 \text{ mm}/\mu\text{s}$. About 4–5 μs was required for this packet to traverse the probe volume. The plots in Fig. 3 were all recorded at the center of the NO packet. Distributions probed

$\pm 1.5 \mu\text{s}$ from the center of the packet were similar to those obtained in the center.

The angular dependence of the NO state distribution on the scattering angle, θ_s , was investigated at $\theta_i = 40^\circ$. Since angular resolution was restricted by the size and distance of the probe volume, only qualitative statements are given. The CID yield was most intense near the specular angle, $\theta_s = \theta_i$. When monitoring NO at $\theta_s = 70^\circ$ ($\theta_i = 40^\circ$) the signal dropped, as did the signal obtained for scattered NO (i.e. the ratio between the NO CID signal and the signal from scattered background NO remained constant). This result suggests that NO $_2^*$ CID on MgO(100) occurs via direct inelastic scattering rather than trapping-desorption.

It is noteworthy that the NO rotational distributions are similar for the cases of NO $_2^*$ CID and NO scattered inelastically from MgO(100) [24], and the degree of spin-orbit excitation is also similar for these two experiments, i.e. the $[^2\Pi_{3/2}]/[^2\Pi_{1/2}]$ ratio is \sim unity. In contrast, in the gas-phase unimolecular decomposition and CID of NO $_2$, significantly colder spin-orbit ratios were observed [23,25]. The difference may be caused by the proximity of the dissociating NO $_2^*$ to the surface. The decomposition lifetimes of NO $_2$ range between 5 and 0.5 ps for excess energies 0–1000 cm^{-1} [26], and if scattered NO $_2$ acquires enough internal energy to cause its unimolecular decomposition rate to be in the subpicosecond regime, it will fragment a few angstrom from the surface. In this case, interaction of the NO product with the surface is inevitable, and the decomposition step cannot be taken as separate from the molecule-surface interaction.

The θ_i dependence of the NO distributions (Figs. 3b and 3c) suggests that the normal component of E_{inc} contributes more to dissociation than does the parallel component. However, for $\theta_i = 45^\circ$, the normal component, E_n , is 970 cm^{-1} (120 meV). This cannot reconcile the observed dissociation features, since after dissociation less than 750 cm^{-1} (93 meV) is available to be distributed among NO internal degrees of freedom and into product c.m. translational energy. Accordingly, the steep drop in Fig. 3c would be expected to appear at lower J'' . Therefore, the observed features are not due exclusively to E_n . The NO $_2^*$ velocity component parallel to the crystal surface could play a role if surface corrugation is taken

into account (maximum corrugation amplitude $\approx 0.40 \text{ \AA}$ [27,28]). Furthermore, energy transfer between the surface and the incident molecules, as well as multiple collisions, should be considered.

In summary, the first observation of CID of NO $_2^*$ on a surface, obtained with state-resolved product detection and control of both internal and translational energies of the incident molecule, is reported. The CID mechanism is established mainly by the similarity of the NO surface-CID yield spectrum, obtained by monitoring selected NO J'' states while varying the pump wavelength, with spectra obtained by LIF of NO $_2$ and gas-phase CID. The preliminary results reported here suggest that CID occurs following direct inelastic scattering rather than trapping-desorption, but that surface interaction may affect the NO state distributions.

Acknowledgement

We thank C.R. Bieler and A. Sanov for valuable discussions. HF thanks the Deutsche Forschungsgemeinschaft for a fellowship and JTS thanks the Department of Education for a fellowship.

References

- [1] B.N.J. Persson and M. Persson, *Surface Sci.* 97 (1980) 609.
- [2] A.O. Bawagan, L.H. Beard, R.B. Gerber and D.J. Kouri, *Chem. Phys. Letters* 84 (1981) 339.
- [3] R.R. Lucchese and J.C. Tully, *J. Chem. Phys.* 80 (1984) 3451.
- [4] G. Rosenblatt, *Accounts Chem. Res.* 14 (1981) 42.
- [5] H. Zacharias, M.M.T. Loy and P.A. Roland, *Phys. Rev. Letters* 49 (1982) 1790.
- [6] J. Misewich, C.N. Plum, G. Blyholder, P.L. Houston and R.P. Merrill, *J. Chem. Phys.* 78 (1983) 4245.
- [7] J. Misewich, P.L. Houston and R.P. Merrill, *J. Chem. Phys.* 82 (1985) 1577.
- [8] J. Misewich, H. Zacharias and M.M.T. Loy, *Phys. Rev. Letters* 55 (1985) 1919.
- [9] E. Kolodney and A. Amirav, in: *Dynamics on surfaces*, Vol. 17, eds. B. Pullman, J. Jortner, A. Nitzan and R.B. Gerber (Reidel, Dordrecht, 1984) p. 231.
- [10] E. Kolodney, A. Amirav, R. Elber and R.B. Gerber, *Chem. Phys. Letters* 111 (1984) 366.
- [11] E. Kolodney, A. Amirav, R. Elber and R.B. Gerber, *Chem. Phys. Letters* 113 (1985) 303.
- [12] R.B. Gerber and A. Amirav, *J. Phys. Chem.* 90 (1986) 4483.

- [13] A. Danon, E. Kolodney and A. Amirav, *Surface Sci.* 193 (1988) 132.
- [14] A. Danon and A. Amirav, *J. Phys. Chem.* 93 (1989) 5549.
- [15] E. Kolodney, D. Bauch, P.S. Powers, H. Reisler and C. Wittig, *J. Chem. Phys.* 90 (1989) 3883.
- [16] P.S. Powers, E. Kolodney, L. Hodgson, G. Ziegler, H. Reisler and C. Wittig, *J. Chem. Phys.* 95 (1991) 8387.
- [17] E. Kolodney, D. Bauch, P.S. Powers, G. Ziegler and H. Reisler and C. Wittig, in: *Mode selective chemistry*, ed. J. Jortner (Kluwer Academic Publishers, Dordrecht, 1991) p. 441.
- [18] E. Kolodney, P.S. Powers, L. Hodgson, H. Reisler and C. Wittig, *J. Chem. Phys.* 94 (1991) 2330.
- [19] U. Robra, H. Zacharias and K.H. Welge, *Z. Physik D* 16 (1990) 175.
- [20] K.O. Patten, J.D. Burley and H.S. Johnston, *J. Phys. Chem.* 94 (1990) 7960.
- [21] O.J. Orient, K.E. Martus, A. Chutjian and E. Murad, *Phys. Rev. A* 45 (1992) 2998, and references cited therein.
- [22] H. Ferkel, L. Hodgson, J.T. Singleton, P.M. Blass, H. Reisler and C. Wittig, submitted for publication.
- [23] C.R. Bieler, A. Sanov, M. Hunter and H. Reisler, *J. Phys. Chem.* 98 (1994) 1058.
- [24] E. Kolodney, D. Bauch, P.S. Powers, H. Reisler and C. Wittig, *Chem. Phys. Letters* 145 (1988) 177.
- [25] M. Hunter, S.A. Reid, D.C. Robie and H. Reisler, *J. Chem. Phys.* 99 (1993) 1093.
- [26] S.I. Ionov, G.A. Brucker, C. Jaques, Y. Chen and C. Wittig, *J. Chem. Phys.* 99 (1993) 3420.
- [27] K.H. Riedler, *Surface Sci.* 118 (1982) 57.
- [28] G. Brusdeylins, R.B. Doak, J.G. Skofronick and J.P. Toennies, *Surface Sci.* 128 (1983) 191.